

# Electronic structures and optical properties of layered perovskites $\text{Sr}_2\text{M O}_4$ ( $\text{M} = \text{Ti}, \text{V}, \text{Cr}$ , and $\text{Mn}$ ): An ab initio study

Hongming Wang,<sup>1</sup> Y. Kawazoe,<sup>1</sup> Xiangang Wan,<sup>2</sup> and Jinming Dong<sup>2</sup>

<sup>1</sup>Institute for Materials Research, Tohoku University, Sendai 980-8577, Japan

<sup>2</sup>Group of Computational Condensed Matter Physics,  
National Laboratory of Solid State Microstructures and Dept. of Physics,  
Nanjing University, Nanjing 210093, P. R. China

(Dated: April 14, 2024)

## Abstract

A series of layered perovskites  $\text{Sr}_2\text{M O}_4$  ( $\text{M} = \text{Ti}, \text{V}, \text{Cr}$ , and  $\text{Mn}$ ) is studied by ab initio calculations within generalized gradient approximation (GGA) and GGA+U schemes. The total energies in different magnetic configurations, including the nonmagnetic, ferromagnetic, the layered antiferromagnetic with alternating ferromagnetic plane and the staggered in-plane antiferromagnetic (AFM-II) order, are calculated. It is found that  $\text{Sr}_2\text{TiO}_4$  is always a nonmagnetic band insulator. For  $\text{Sr}_2\text{MnO}_4$ , both GGA and GGA+U calculations show that the insulating AFM-II state has the lowest total energy among all the considered configurations. For  $\text{M} = \text{V}$  and  $\text{Cr}$ , the GGA is not enough to give out the insulating AFM-II states and including the on-site electron-electron correlation effect  $U$  is necessary and efficient. The AFM-II state will have the lowest total energy in both cases when  $U$  is larger than a critical value. Further, the optical conductivity spectra are calculated and compared with the experimental measurements to show how well the ground state is described within the GGA or GGA+U. The results indicate that  $U$  is overestimated in  $\text{Sr}_2\text{VO}_4$  and  $\text{Sr}_2\text{CrO}_4$ . To make up such a deficiency of GGA+U, the contributions from proper changes in the ligand field, acting cooperatively with  $U$ , are discussed and shown to be efficient in  $\text{Sr}_2\text{CrO}_4$ .

PACS numbers: 71.27.+a, 71.30.+h, 78.20.-e

## I. INTRODUCTION

Perovskite transition-metal oxides have been intensively studied<sup>1</sup> due to their various intriguing physical properties, such as the ferroelectricity, complex charge, spin and/or orbital order, and some combined properties including magnetoelectric multiferroics<sup>2</sup> and colossal magnetoresistance.<sup>3</sup> In this family, the two-dimensional layered perovskite in  $K_2NiF_4$  structure is particularly interesting because of the high- $T_c$  superconductivity in cuprates based on  $La_2CuO_4$  and the novel charge, spin, and/or orbital stripes in nickelates and manganites.<sup>4</sup> Compared with the quite early success in the synthesis of  $ABO_3$  like perovskites, only recently has a series of layered perovskites  $Sr_2MO_4$  with transition-metal  $M = Ti, V, Cr, Mn$ , and  $Co$  been successfully synthesized in single-crystalline thin films.<sup>5</sup> Thus, the variation of their electronic structures could be systematically studied as the occupation of d orbitals increases from empty ( $d^0$  for  $Ti^{4+}$ ) to half-filled ( $d^5$  for  $Co^{4+}$ ).<sup>5</sup> In the  $d^0$  case,  $Sr_2TiO_4$  is always a nonmagnetic insulator. For  $M = V$ , the surrounding elongated octahedral crystal field is thought to make the single  $d^1$  electron stay in the doubly degenerate  $d_{xz+yz}$  orbitals and thus result in metallic features, but experimentally  $Sr_2VO_4$  is found to be an antiferromagnetic (AFM) insulator.<sup>5</sup> Since the singly occupied degenerate  $d_{xz+yz}$  orbitals are active in the orbital degree of freedom, a kind of spin and/or orbital ordering<sup>5,6</sup> has been proposed to explain its insulating AFM ground state. In the  $M = Cr$  case, two d electrons are supposed to occupy the doubly degenerate  $d_{xz+yz}$  orbitals and are expected to be a simple Mott-Hubbard insulator in stark contrast to the metallic cubic perovskite  $SrCrO_3$ .<sup>7</sup> Ignoring the empty  $e_g$  orbitals,  $Sr_2CrO_4$  has a dual relation to  $Sr_2RuO_4$ , which has two holes instead of two electrons in the narrow  $t_{2g}$  orbitals and possesses superconductivity.<sup>8</sup> Three d electrons in  $Sr_2MnO_4$  will fully occupy the lower Hubbard bands of the  $t_{2g}$  orbitals, making the system an AFM insulator. All the systems above only have  $t_{2g}$  electrons in the states around the Fermi level, but for  $M = Co$  it is totally different from the others by having electrons in the  $e_g$  orbitals and possessing metallic FM orders.<sup>5,9</sup> All these systematical variations of electronic structures are revealed by optical conductivity measurements.<sup>5</sup> The anisotropy of the polarized optical conductivity due to the two-dimensional  $MO_2$  sheets in the layered perovskite structures is also clearly shown by measurements with  $E \parallel c$  and  $E \parallel ab$ , respectively.

Though it is now found quite difficult to predict the correct spin and orbital state in the  $t_{2g}$  system and more and more researchers agree that methods beyond the local density

approximation (LDA) seem to be necessary, the conventional description within the LDA and LDA+U is still important and key as basic knowledge prior to the other methods.<sup>10</sup>  $\text{Sr}_2\text{VO}_4$  has been already carefully investigated by first-principles calculations<sup>11,12</sup> within local spin density approximation (LSDA). But the LSDA calculation failed in reproducing its AFM insulator state, and a +U calculation has not been tried. To the best of our knowledge, no first-principles calculations have been performed on  $\text{Sr}_2\text{CrO}_4$  so far. Wang et al.<sup>13</sup> studied  $\text{Sr}_2\text{MnO}_4$  just within the LSDA and found it is an AFM insulator. For  $\text{Sr}_2\text{CoO}_4$ , both LSDA and LSDA+U calculations<sup>9,14</sup> can successfully describe this system and show that the strong hybridization between the Co 3d and O 2p orbitals makes this  $d^5$  system a ferromagnetic (FM) metal. Therefore, in this paper, we put emphasis on the so called  $t_{2g}$  system with  $M = \text{V}, \text{Cr}, \text{Mn}$  and will not cover  $\text{Sr}_2\text{CoO}_4$  again. We use the generalized gradient approximation (GGA) instead of the LSDA in order to improve the accuracy for spin-polarized calculation.<sup>15</sup> The on-site electron-electron correlation effect  $U$  is also taken into account for these systems. To make a complete theoretical research and comparison, various magnetic configurations for each case are studied. Though the three-dimensional ferromagnetism and layered AFM state with alternating ferromagnetic  $\text{MO}_2$  sheets (AFM-I) have been ruled out by experimental measurements on thin-film samples,<sup>5</sup> both of them are calculated here. In layered perovskite structure, the typical and simplest magnetic configuration, staggered in-plane AFM order (AFM-II),<sup>16</sup> is also included, which is the most important configuration for understanding the underlying physics in these systems despite the fact that some other complex spin and/or orbital orderings may exist in the  $M = \text{V}$  or  $\text{Cr}$  case.<sup>5,6</sup>  $U$  is found to play an important role in both  $\text{Sr}_2\text{VO}_4$  and  $\text{Sr}_2\text{CrO}_4$  where the GGA is insufficient for predicting the AFM insulating ground states. The effects of the changes in ligand field, which might influence the  $U$  value, are also discussed. Finally, the optical conductivity spectra are calculated and compared with the experimental measurements to show the efficiency of the GGA and GGA+U schemes in describing these systems.

## II. METHODOLOGY

The Vienna ab initio simulation package (VASP) plane-wave code<sup>17</sup> has been employed in our calculations. The projector augmented-wave (PAW) version of pseudopotential<sup>18</sup> is used to describe the electron-ion interaction. The exchange correlation term is treated within the

GGA as parametrized by Perdew et al.<sup>15</sup> The approach of Dudarev et al. for adding  $U$  is used in the GGA+ $U$  calculation, in which only one effective on-site Coulomb interaction parameter is needed.<sup>19</sup> For all  $\text{Sr}_2\text{M O}_4$ , the lattice constants are taken from experimental measurements of thin-film samples<sup>5</sup> as shown in Table I. There is an orthorhombic deviation from tetragonal symmetry in each case. The largest distortion is in the  $\text{M} = \text{Cr}$  case with  $a=b=1.023$ . In the other cases,  $a=b$  are all nearly 1.0. In the first approximation,<sup>9</sup> such an orthorhombic deviation from tetragonal symmetry is ignored and all are assumed to have typical  $\text{K}_2\text{NiF}_4$  structure in our calculation. The internal atomic coordinates are fully optimized until the force on the atom is less than 0.002 eV/Å. For simulating the AFM-II state, a cell as large as  $\frac{p}{2} \times \frac{p}{2} \times 1$  of the conventional  $\text{K}_2\text{NiF}_4$  unit cell is needed, which is also used for other states in order to accurately compare their total energies.

The interband optical responses are calculated within the electric-dipole approximation using the Kubo formula<sup>20</sup> implemented by Furthmüller,<sup>21</sup> in which the imaginary part of the dielectric function can be expressed as

$$\epsilon_2(\omega) = \frac{8\pi e^2}{\omega^2 m^2 V} \sum_{c,v,k} \langle c; k | \hat{p} | v; k \rangle \langle v; k | \hat{p} | c; k \rangle \delta(E_c(k) - E_v(k) - \hbar\omega);$$

where  $c$  and  $v$  represent the conduction and valence bands, respectively.  $|c; k\rangle$  ( $|v; k\rangle$ ) and  $E_c$  ( $E_v$ ) are the eigenstate and eigenvalue of the conduction (valence) band obtained from VASP calculations, respectively.  $\hat{p}$  is the momentum operator,  $\hat{e}$  is the electric field vector of the incident photon, denoting polarization of the light, and  $\omega$  is its frequency. An  $8 \times 8 \times 8$  grid is used to sample the Brillouin zone for integration over  $k$  space with the linear tetrahedron scheme improved by Blochl et al.<sup>22</sup> The energy cutoff of the plane wave is 520 eV. The convergence on  $k$  points and energy cutoff is carefully checked.

### III. RESULTS AND DISCUSSIONS

#### A. $\text{Sr}_2\text{TiO}_4$

The lattice constants of the  $\text{Sr}_2\text{M O}_4$  are taken from the experimental measurements and only the internal positions of the apical oxygen ( $\text{O}_a$ ) and the Sr atoms are needed to be relaxed due to the symmetry of the crystal structure. The obtained results are listed in Table I for  $\text{Sr}_2\text{TiO}_4$  together with  $\text{M} = \text{V}, \text{Cr}$ , and  $\text{Mn}$ . For  $\text{Sr}_2\text{TiO}_4$ , the internal positions of

TABLE I: The lattice constants taken from the experimental measurements and the theoretically optimized internal coordinates relative to the c lattice for the apical oxygen ( $O_a$ ) and Sr atoms.  $J = d_c/d_{ab}$  is the Jahn-Teller distortion degree with  $d_c$  ( $d_{ab}$ ) being the M-O bond length along the c axis (in the ab plane). The length unit is in angstroms.

|          | Ti      | V       | Cr      | Mn      |
|----------|---------|---------|---------|---------|
| a        | 3.866   | 3.832   | 3.756   | 3.755   |
| c        | 12.60   | 12.59   | 12.59   | 12.62   |
| $O_a$    | 0.15950 | 0.15781 | 0.15899 | 0.15858 |
| Sr       | 0.14589 | 0.14486 | 0.14673 | 0.14646 |
| $d_{ab}$ | 1.93    | 1.92    | 1.88    | 1.88    |
| $d_c$    | 2.01    | 1.99    | 2.00    | 2.00    |
| J        | 1.041   | 1.036   | 1.063   | 1.063   |

$O_a$  and Sr are 0.159 50 and 0.145 89, being comparable with those obtained by other LDA calculations,<sup>23</sup> 0.160 and 0.145, respectively. In all cases, the oxygen octahedron surrounding the M ion has a similar Jahn-Teller (JT) distortion with an elongation along the c axis. The distortion degree is defined as  $J = d_c/d_{ab}$  with  $d_c$  ( $d_{ab}$ ) being the M-O bond length along the c axis (in the ab plane), as listed in Table I. Among them,  $M = Cr$  and  $Mn$  have the largest distortion and  $M = V$  has the smallest.

The  $Sr_2TiO_4$  system is quite simple. It is a band insulator as shown by the density of states (DOS) in Fig. 1. The valence and conduction bands are mostly composed of the oxygen 2p and Ti 3d bands, respectively. The width of the  $t_{2g}$  bands is much narrower than that of the  $e_g$  bands because of their different bonding type with the oxygen p bands. The in-plane  $d_{xy}$  and  $d_{x^2-y^2}$  bands are wider than the out-of-plane  $d_{xz+yz}$  and  $d_{3z^2-r^2}$  bands, respectively, due to the elongated oxygen octahedra, which also make the in-plane oxygen p bands wider than that of the apical one. The calculated polarized optical conductivity spectra with electric field  $E$  parallel ( $E_{||c}$ ) and perpendicular ( $E_{\perp c}$ ) to the c axis are shown in Fig. 1 (a). The experimental spectra<sup>5</sup> are also plotted for easy comparison. Obviously, the calculated optical gap is underestimated due to the well-known shortcomings of the GGA.<sup>24</sup> The anisotropy of the spectra originating from the two-dimensional layered structure is also observed. The shoulder near 3.0 eV in the calculated  $E_{||c}$  spectrum is contributed by

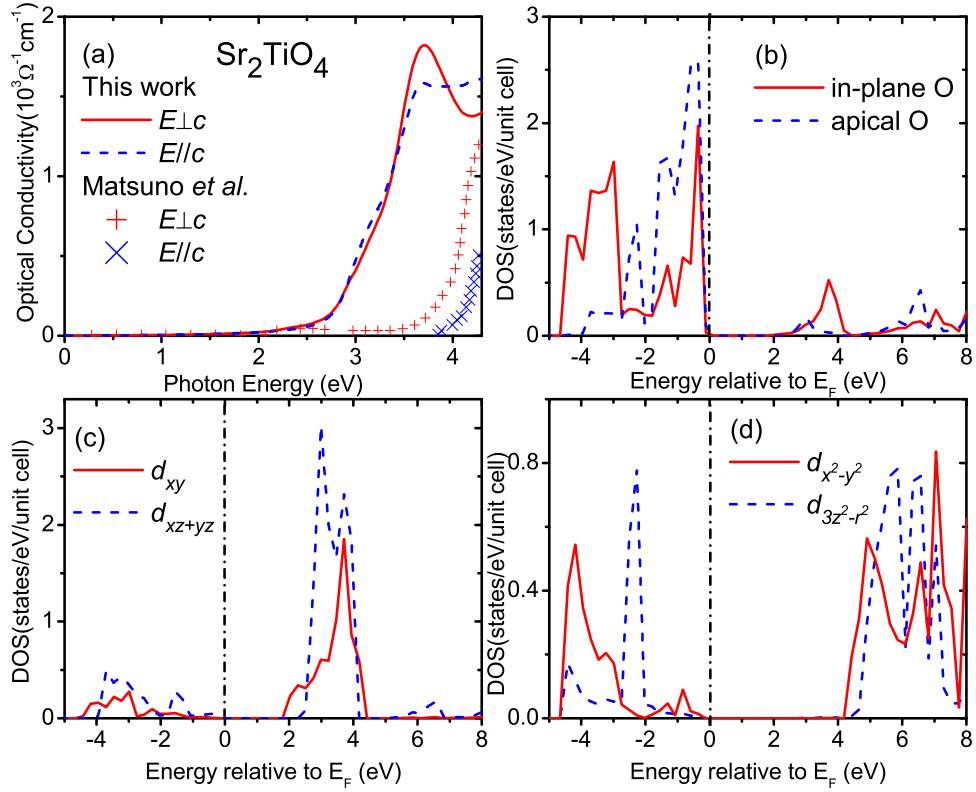


FIG. 1: (Color online) Calculated results within the GGA for  $\text{Sr}_2\text{TiO}_4$ . (a) Optical conductivity spectra (lines), (b) projected partial DOS for in-plane (solid) and apical (dashed) oxygen 2p bands, and (c)  $t_{2g}$  and (d)  $e_g$  bands of the Ti 3d electrons. In (a), the experimental spectra (symbols, Ref. 5) are plotted in symbols. The vertical dash-dotted line indicates the Fermi energy level.

transitions from the occupied apical oxygen 2p bands to the empty  $d_{xz+yz}$  orbitals centered around 3.0 eV above the Fermi level. Such a kind of transition is not observed when  $E \parallel c$ . In both the  $E \parallel c$  and  $E \perp c$  cases, the first high peak around 3.7 eV is attributed to the transition from in-plane and apical oxygen 2p orbitals to the Ti  $d_{xy}$  and  $d_{xz+yz}$  orbitals, respectively. When  $E \parallel c$ , this peak is quite broader since, just below the Fermi level, the apical oxygen p DOS structure is wider than that of the in-plane oxygen, as shown in Fig. 1(b).

## B. $\text{Sr}_2\text{VO}_4$

The experimental parameters for  $\text{O}_a$  and Sr in  $\text{Sr}_2\text{VO}_4$  are 0.157 78 and 0.145 62,<sup>25</sup> respectively, comparable with our GGA results, 0.157 81 and 0.144 86.  $\text{Sr}_2\text{VO}_4$  has the smallest JT distortion among all the systems. In order to search for the possible ground

TABLE II: The calculated total energies of  $\text{Sr}_2\text{M O}_4$  in NM, AFM-I and AFM-II states within GGA. All the energies are given in relative to that of FM state and the unit is meV/cell.

|        | V   | Cr   | Mn   |
|--------|-----|------|------|
| NM     | 280 | 1252 | 3312 |
| AFM-I  | -6  | -29  | -38  |
| AFM-II | 280 | 297  | -629 |

state for  $\text{M} = \text{V}, \text{Cr},$  and  $\text{Mn}$ , we have calculated the total energies of the optimized structure in various magnetic configurations. The obtained total energy relative to the FM state by GGA calculations is shown in Table II. For  $\text{M} = \text{V}$ , the AFM-I state has the lowest energy, which is inconsistent with the experimental analysis since the FM order in the ab plane would give rise to the metallic optical conductivity when  $E \geq c$ . In the left panel of Fig. 2, the total DOS of  $\text{Sr}_2\text{VO}_4$  in the AFM-I state clearly shows metallic features. In the picture of JT-distortion, the doubly degenerate  $d_{xz+yz}$  orbitals are lower than the  $d_{xy}$  orbital, but all of them have contributions to the DOS at the Fermi level although there is only one valence d electron. This is very similar to that in the  $d^4$  system of  $\text{Sr}_2\text{RuO}_4$ .<sup>26</sup> It should be mentioned that in  $\text{Sr}_2\text{VO}_4$ , though the AFM-II configuration is initialized for calculations, the electronic charge density always converges to the NM state and the AFM-II state can not be achieved in our GGA calculation. In Table II, the AFM-II energy for  $\text{M} = \text{V}$  is in fact that of the NM state. Pickett et al. also tried in LSDA calculations to search for the AFM state of  $\text{Sr}_2\text{VO}_4$  but failed.<sup>11</sup>

For a d-electron system, usually the strong electron-electron correlation  $U$  is included in order to remedy the deficiency of the GGA. In addition,  $U$  had been used for predicting the correct energy order in the  $t_{2g}$  system  $\text{YTiO}_3$ , where the GGA failed.<sup>27</sup> In order to determine the proper value of  $U$ , a series of calculations on different magnetic states for  $\text{Sr}_2\text{VO}_4$  with different  $U$  have been performed. The variations of total energies in different configurations relative to the FM state when  $U$  is increased are plotted in the left panel of Fig. 3. The AFM-I state is almost degenerate with the FM one, indicating that the coupling between the  $\text{VO}_2$  sheets is very small. The total energy of the AFM-II state is the lowest when  $U$  is larger than a critical value  $U_c$ , about 2.08 eV.

The evolution of the  $t_{2g}$  DOS with increasing the  $U$  parameter in the AFM-II state for

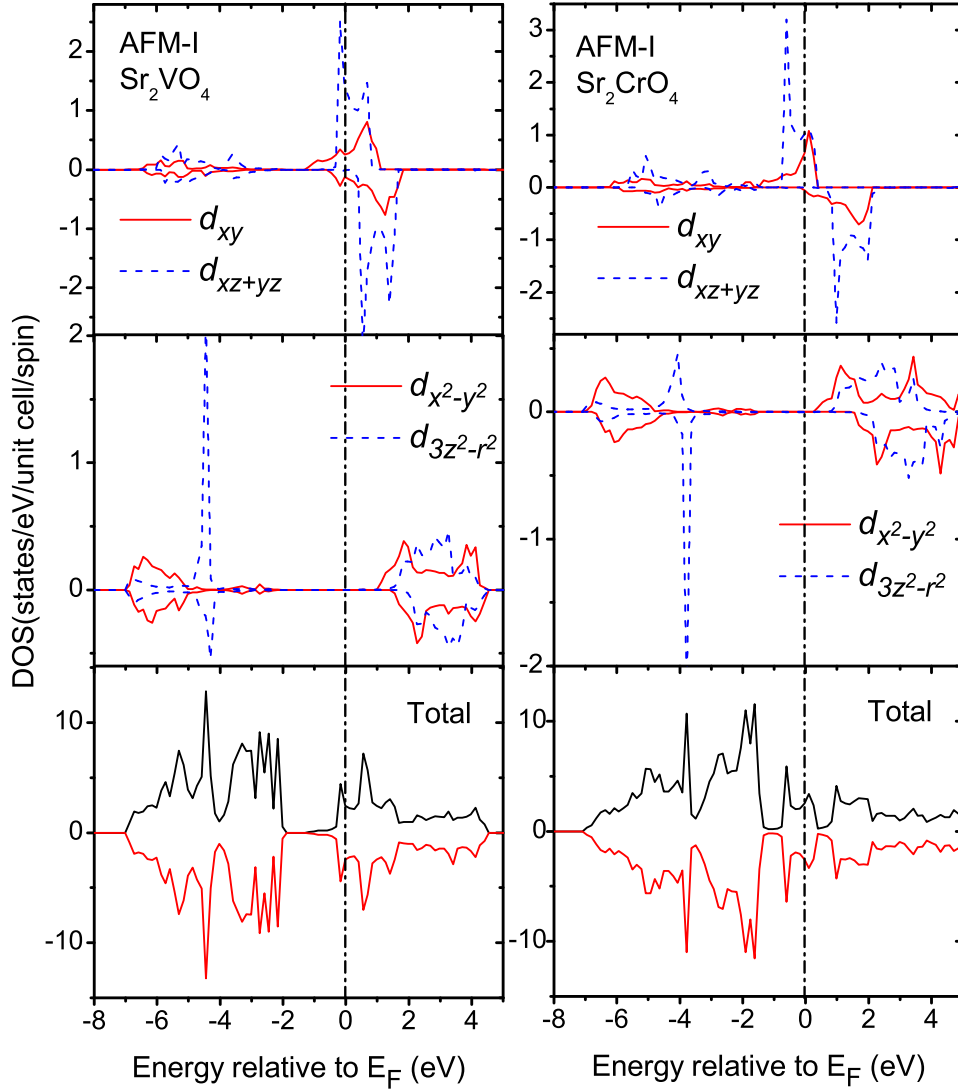


FIG. 2: (color online) The calculated DOS of the AFM-I state for  $M = V$  (left panel) and  $Cr$  (right panel) within the GGA. The vertical dash-dotted line indicates the Fermi energy level.

$M = V$  is plotted in the left panel of Fig. 4. As  $U$  increases, the occupation of the  $d$  electron on the  $V$  ion site will be slowly shifted from the  $d_{xz+yz}$  to the  $d_{xy}$  orbital. Due to the separation of  $d_{xy}$  from  $d_{xz+yz}$ , a metal-to-insulator transition happens near  $U = 2.0$  eV. The  $d$  electron eventually occupies the spin-up  $d_{xy}$  orbital instead of the doubly degenerate  $d_{xz+yz}$  orbitals though the latter should be lower in energy according to the picture of elongated JT distortion. This kind of occupancy will destroy any possible orbital ordering although recently Imai et al. proposed a kind of spin and orbital order in this system.<sup>6</sup> In fact, in the FM state, the doubly degenerate  $d_{xz+yz}$  orbitals occupied by one  $d$  electron will cause FM



instability as found by Pickett et al.<sup>11</sup>

Since the Neel temperature of  $\text{Sr}_2\text{VO}_4$  is reported to be about 47 K,<sup>28</sup> the energy difference between the AFM-II and FM states should not be too large if using the popular spin-1/2 two-dimensional Heisenberg model to estimate the Neel temperature.<sup>29</sup> Therefore, in the calculation of optical conductivity spectra we roughly take the  $U$  value of 2.1 eV, which is slightly larger than the critical value. The obtained optical conductivity spectra as well as the experimental ones are shown in Fig. 5 together with partial DOS for oxygen and V. From the DOS, it can be seen that the fundamental gap is about 0.1 eV, but the optical gap, obtained from the calculated optical conductivity spectra, is as high as about 2.0 eV. Obviously, the transitions between the occupied  $d_{xy}$  orbital and the empty  $d_{xz+yz}$  orbitals, which constitute the fundamental gap, are forbidden for both  $E \parallel c$  and  $E \parallel ab$ . This is reasonable and consistent with the optical selection rule of  $d \rightarrow d$  transitions.<sup>30</sup> According to this rule, in the AFM-II configuration, the transition from the occupied spin-up  $d_{xy}$  orbital to the nearest unoccupied spin-up  $d_{xy}$  one is allowed only for  $E \parallel c$ , which is the so-called Mott-Hubbard transition.<sup>5</sup> Clearly, such a kind of transition contributes to the 2.0 eV optical gap and the shoulder around 2.75 eV in the calculated  $E \parallel c$  spectrum. However, both the optical gap and the transition energy are overestimated by using such a large  $U$  of 2.1 eV as compared with the experimentally suggested value 1.0 eV as indicated by the peak around 1.0 eV in the experimental  $E \parallel c$  spectrum.<sup>5</sup> The peak around 3.0 eV in the calculated spectrum for  $E \parallel c$  can be attributed to the transition from the in-plane oxygen 2p bands to the empty  $d_{xz+yz}$  orbitals. This peak corresponds to the experimental one also near 3.0 eV, which is called the charge transfer gap.<sup>5</sup> When  $E \parallel ab$ , due to the existence of SrO layers, the intersite  $d \rightarrow d$  Mott-Hubbard transition is negligible and not seen. The charge transfer gap in this case is due to the transition from the apical oxygen 2p bands to the  $d_{xz+yz}$  orbitals. The resulting broad and multippeak structure around 3.0 eV in the calculated spectrum is a little lower than the corresponding experimental one.

#### C. $\text{Sr}_2\text{CrO}_4$

The optimized internal position parameters for O<sub>a</sub> and Sr in  $\text{Sr}_2\text{CrO}_4$  are 0.158 99 and 0.146 73, respectively.  $\text{Sr}_2\text{CrO}_4$  has a larger JT distortion than  $\text{Sr}_2\text{VO}_4$ . Within the GGA, it has similar results as  $\text{Sr}_2\text{VO}_4$  does. The AFM-I state has the lowest total energy, and its

DOS shown in right panel of Fig. 2 also possesses metallic features. Similar to  $\text{Sr}_2\text{VO}_4$  and  $\text{Sr}_2\text{RuO}_4$ , both  $d_{xy}$  and doubly degenerate  $d_{xz+yz}$  orbitals have contributions to the DOS at Fermi level. In  $\text{Sr}_2\text{CrO}_4$ , the Fermi level is a little higher than that in  $\text{Sr}_2\text{VO}_4$  due to one more d electron.

As done in  $\text{Sr}_2\text{VO}_4$ , the electron-electron correlation effect  $U$  is taken into account and the total energy dependence on the  $U$  value in various magnetic configurations is plotted in the right panel of Fig. 3. The energy difference between the AFM -I and FM state is quite larger than that in  $\text{Sr}_2\text{VO}_4$ . It seems that the coupling between  $\text{CrO}_2$  sheets is quite stronger than that between  $\text{VO}_2$  ones. When  $U$  is larger than the critical value  $U_c$ , about 3.36 eV, the total energy of AFM -II state is the lowest among all the states. In the right panel of Fig. 4, the variation of Cr  $t_{2g}$  partial DOS with  $U$  is also plotted. Different from that in  $\text{Sr}_2\text{VO}_4$ , as  $U$  increases, the two d electrons on the  $\text{Cr}^{4+}$  ion will occupy the  $d_{xz+yz}$  orbital more and more, and eventually the  $d_{xy}$  orbital is left empty. The metal-insulator transition will happen at a higher  $U$  value of about 5.0 eV (not shown here), where the  $d_{xy}$  orbital is totally separated from the  $d_{xz+yz}$ . Here, the  $d_{xz+yz}$  orbitals are lower than the  $d_{xy}$ , which is consistent with the picture of the elongated JT distortion in the oxygen octahedron. Therefore, in the  $M = V$  and  $Cr$  cases, the effects of JT distortion and  $U$  are totally different. In the former case,  $U$  acts against the JT distortion, while in the latter case, they work cooperatively. This can also be seen from the forces on the apical oxygen atoms. Before the metal-insulator transition, as the  $U$  increases, the apical oxygen atoms in the  $M = V$  case will feel an increasing attenuating force, while for  $M = Cr$ , the force is going to elongate the octahedron. Thus, in these two systems, the subtle balance of competition between the electron-electron correlation and the electron-lattice interaction may be a key factor to determine their physical properties.

In order to show the cooperative effect of the JT distortion and  $U$  in  $\text{Sr}_2\text{CrO}_4$ , we fixed  $d_{ab}$  and artificially elongated the oxygen octahedron to a degree with  $J = 1.14$ . Again, the total energies of various magnetic configurations relative to the FM one with different  $U$  values are shown in Fig. 6. Obviously, the AFM -II state becomes the most stable when  $U$  is larger than the  $U_c$  value of 2.74 eV, which is smaller than the original one of 3.36 eV. Due to the cooperation of JT distortion, the metal-insulator transition is speeded up with the increasing of  $U$ . The splitting of the triply degenerate  $t_{2g}$  orbital is key to such a transition and the realization of an AFM -II insulator state for both  $\text{Sr}_2\text{VO}_4$  and  $\text{Sr}_2\text{CrO}_4$ .

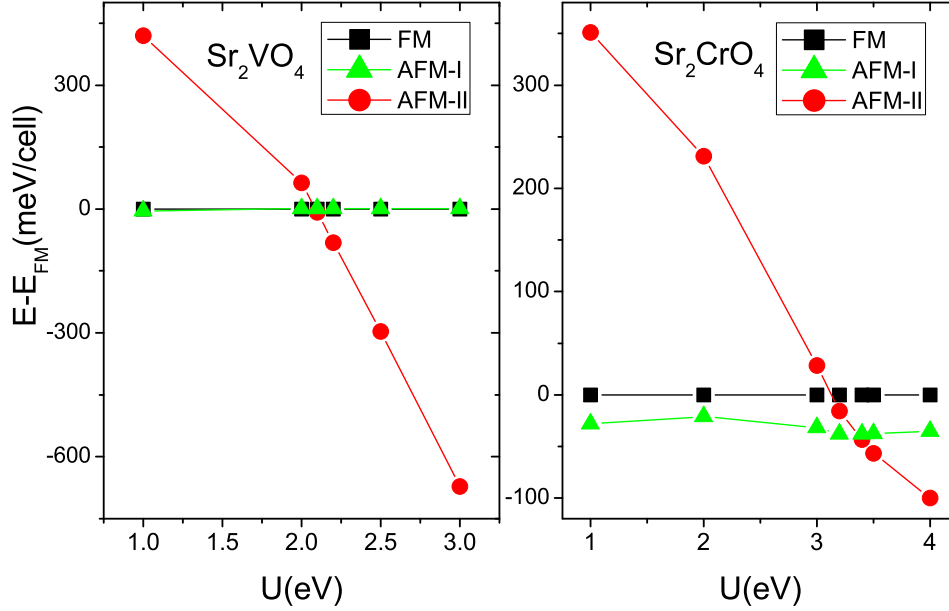


FIG. 3: (Color online) The variations of the total energies relative to the FM state with the  $U$  parameter for  $M = V$  (left panel) and  $Cr$  (right panel).

Other kind of lattice distortions, such as the rotation and/or tilting of oxygen octahedra, which may cause the lattice deviation from the tetragonal symmetry,<sup>31</sup> can also induce the energy splitting in  $t_{2g}$  orbitals and encourage orbital polarization and hence be another driving force of the metal-insulator transition. Here, it is noticed in the  $M = V$  case that the lattice constants are in good agreement between the bulk and film samples and the theoretical  $O_a$  position is almost the same as the bulk sample. The measured  $a$  and  $b$  lattice constants are nearly equal, and the tetragonal symmetry is well kept. This means that  $Sr_2VO_4$  has no obvious orthorhombic distortion and a contribution from the additional ligand field changes is unlikely. In the  $M = Cr$  case, the orthorhombic strain, defined as  $(b-a)/(a+b)$ , is about 0.0112 in the samples, which is quite large and comparable with that in  $Ca_2RuO_4$ , on average being 0.01225.<sup>31</sup> Then, for  $M = Cr$ , the lattice distortions are expected to have a large influence on its magnetic properties. But further investigation of these effects needs more detailed geometric information, which is not available now probably due to the difficulty in the synthesis of samples in bulk. In the similar layered system  $Ca_{2-x}Sr_xRuO_4$ , Z. Fang et al. has demonstrated that the detailed crystal structure is crucial for interpretation of its magnetic phase diagram and orbital physics.<sup>32</sup>

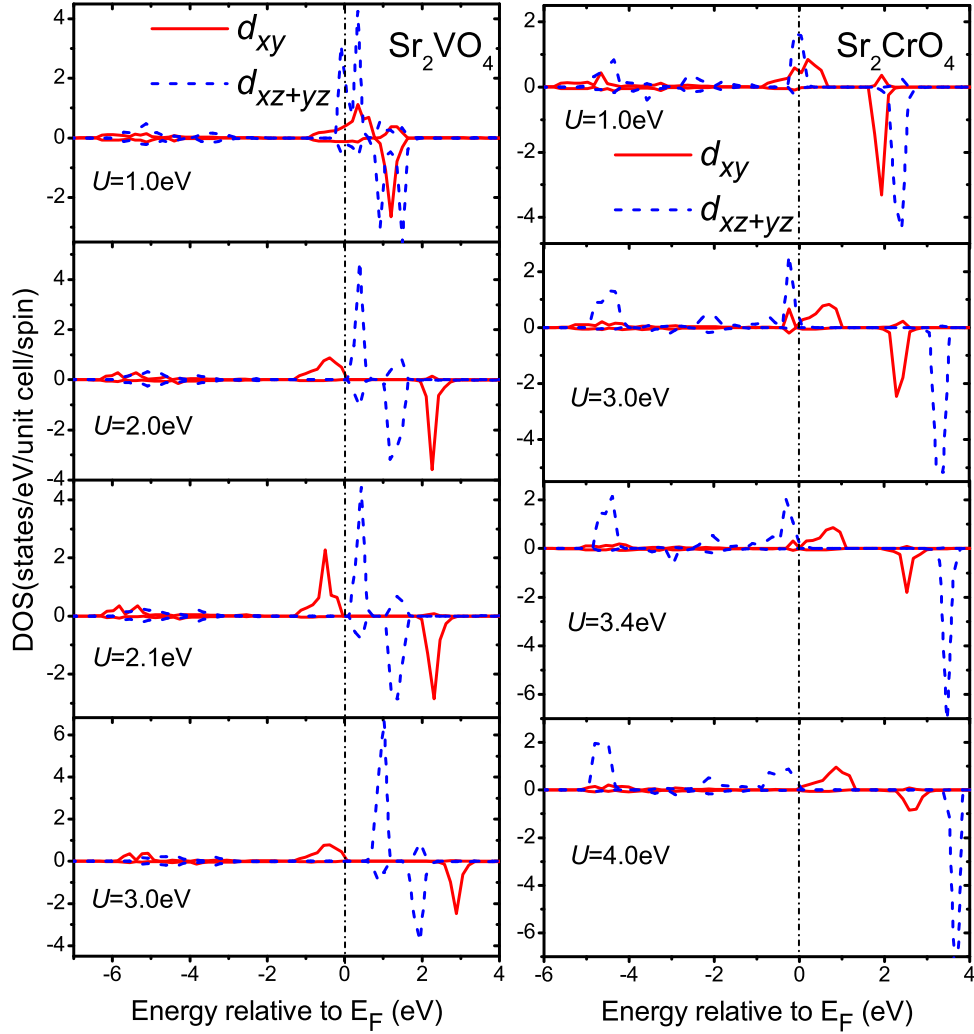


FIG. 4: (Color online) The variations of the  $t_{2g}$  density of states in the AFM -II state with the  $U$  parameter for  $M = V$  (left panel) and  $Cr$  (right panel). The vertical dash-dotted line indicates the Fermi energy level.

Similar to  $Sr_2VO_4$ , for  $M = Cr$ , the  $U$  value of 3.4 eV is taken for the optical conductivity calculation to ensure that the AFM -II state is the lowest in energy and the energy difference from the FM state is not too large, though at this  $U$  value, there is a small weight of DOS at the Fermi level. The theoretical and experimental optical conductivity spectra are shown in Fig. 7. Despite the metallic DOS feature, the obtained optical conductivity spectra with both EPC and EKC look like to have semiconducting features. One of the reasons for this is that the contribution from the phenomenological Drude component is not included in our calculation.<sup>9</sup> The second one is the optical selection rule. According to this rule, the

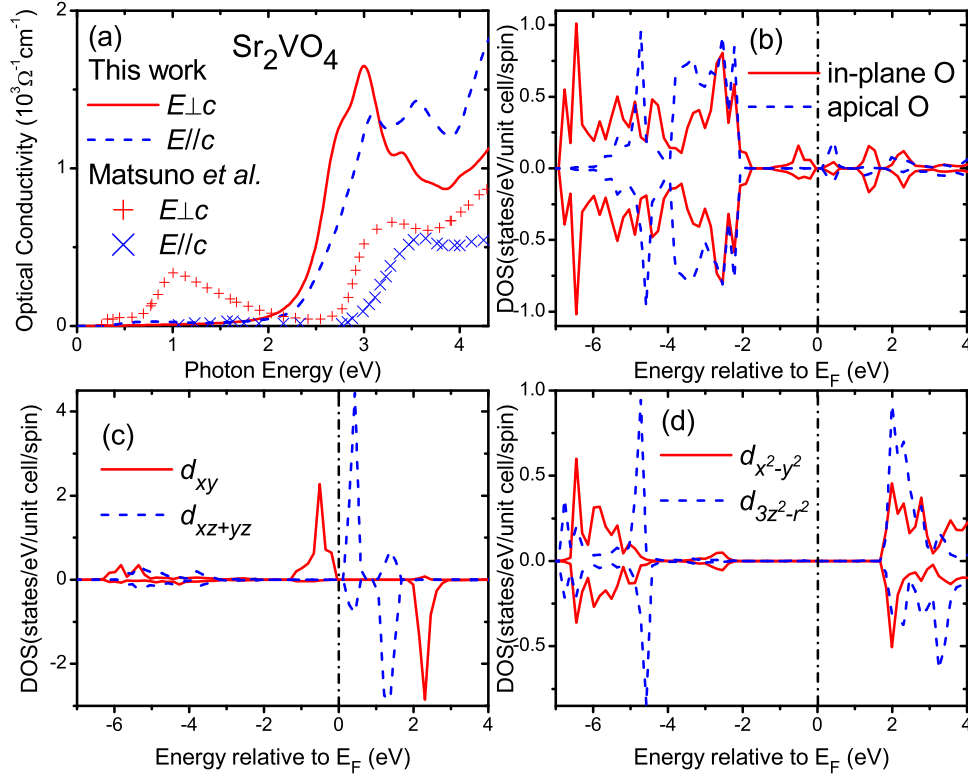


FIG. 5: (color online) (a) The experimental (symbols, Ref. 5) and calculated optical conductivity spectra (lines) for  $\text{Sr}_2\text{VO}_4$  in the AFM-II state with  $U = 2.1$  eV and the corresponding partial DOS for (b) in-plane (solid line) and apical (dashed line) oxygen 2p bands and (c)  $t_{2g}$  and (d)  $e_g$  bands of V 3d electrons. The vertical dash-dotted line indicates the Fermi energy level.

optical transition from occupied  $d_{xz+yz}$  to unoccupied  $d_{xy}$  is forbidden though the eigenvalue difference between them is very small. In the case of  $E_{\parallel c}$ , intersite  $d-d$  transitions can occur and contribute to the peak near 3.5 eV, which could be explained by the  $d_{xz+yz}$  DOS in Fig. 7(c). The position of this peak is quite different from the experimental analysis, where the peak around 1.0 eV is attributed to such a Motz-Hubbard transition.<sup>5</sup> The overestimation of this peak originates from the  $U$  value of 3.4 eV used in the calculation, which locates the unoccupied upper Hubbard bands  $d_{xz+yz}$  as high as about 3.5 eV. The quite broad peak around 2.5 eV in the calculated  $E_{\parallel c}$  spectrum comes from the so-called charge transfer transition between the in-plane oxygen 2p bands near -1.0 eV and the empty  $d_{x^2-y^2}$  orbital at 1.5 eV. However, in the corresponding experimental spectrum, such a peak is around 2.0 eV. When  $E_{\perp c}$ , in the calculated spectrum, the so-called charge transfer transition is around 3.5 eV, which comes from the transitions between apical oxygen 2p and Cr  $d_{3z^2-r^2}$  orbitals.

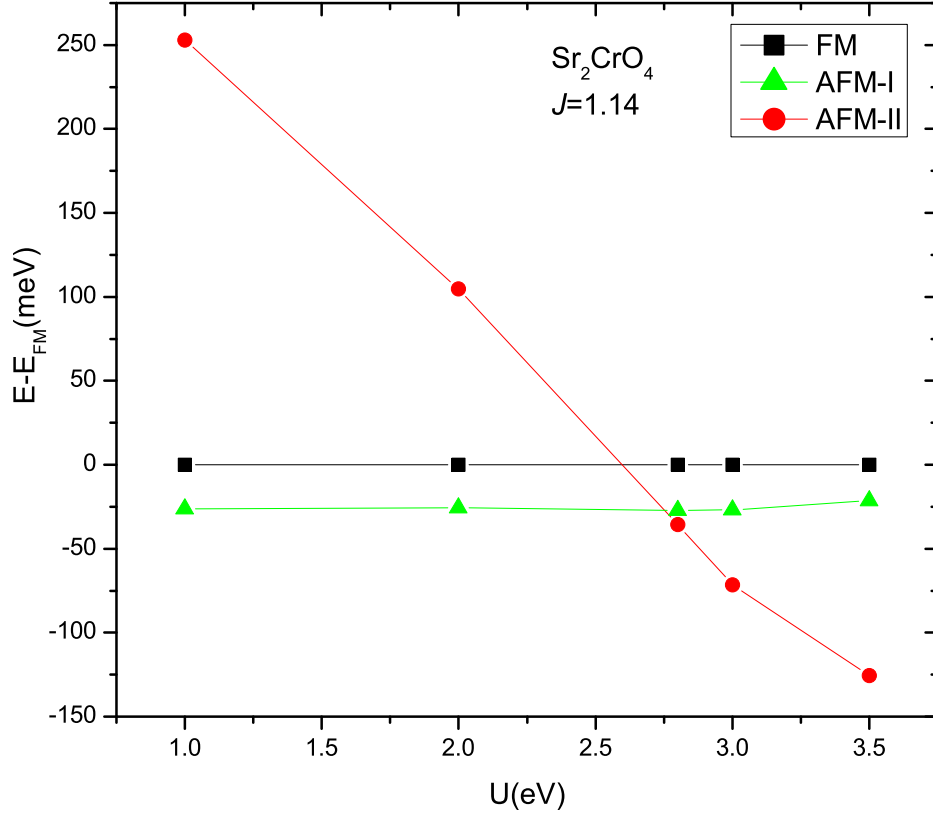


FIG. 6: (color online) The variation of the total energy relative to the FM state with the  $U$  parameter for  $M = Cr$  with the JT distortion of  $J = 1.14$ .

This peak position is also higher than the corresponding experimental value by about 1.0 eV.

Therefore, compared with the experimental measurements,<sup>5</sup> the calculated optical conductivity spectra of  $Sr_2VO_4$  and  $Sr_2CrO_4$  are not good enough due to the overestimation of the  $U$  parameter. As discussed above, just taking into account the electron-electron correlation is not enough to give a good description of the correct ground states of  $Sr_2VO_4$  and  $Sr_2CrO_4$ . Some other factors, such as the possible complex spin and/or orbital ordering and the proper changes of electron-lattice interaction, may be expected to make up the deficiency, or even methods beyond the conventional LDA and LDA +  $U$  are needed. In the  $M = V d^1$  case, we have discussed that the contribution from the additional ligand field is unlikely. With an approach combining the path-integral renormalization group method with LDA calculations, Imai et al. obtained a kind of AFM insulating state consistent with the

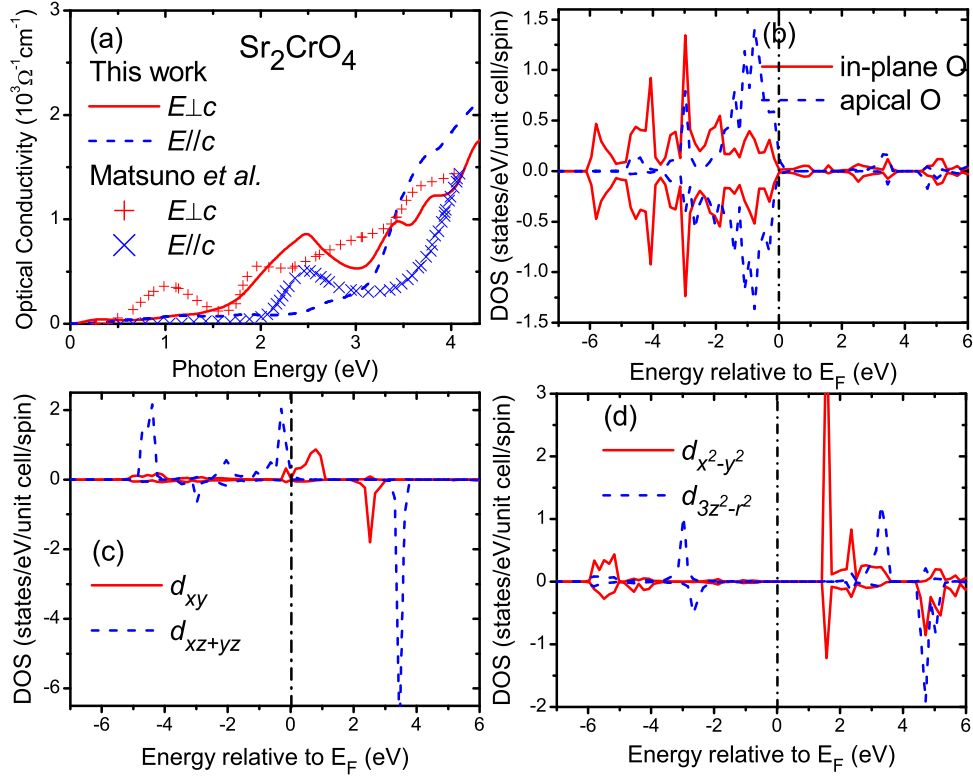


FIG. 7: (color online) (a) The experimental (symbols, Ref. 5) and calculated optical conductivity spectra (lines) for  $\text{Sr}_2\text{CrO}_4$  in the AFM -II state with  $U = 3.4 \text{ eV}$  and the corresponding partial DOS for (b) in-plane (solid line) and apical (dashed line) oxygen 2p bands and (c)  $t_{2g}$  and (d)  $e_g$  bands of Cr 3d electrons. The vertical dash-dotted line indicates the Fermi energy level.

experiments and predicted a nontrivial orbital-stripe order in  $\text{Sr}_2\text{VO}_4$ ,<sup>6</sup> while for  $M = \text{Cr}$ , the  $d^2$  system, the electron-lattice contribution is still possible. As shown in Fig. 6, the simple JT distortion is demonstrated to be quite efficient although this may not be the real distortion in samples.

#### D. $\text{Sr}_2\text{MnO}_4$

The optimized structure parameter for  $\text{Sr}_2\text{MnO}_4$  is 0.158 58 and 0.146 46 for  $\text{O}_a$  and Sr. In the  $M = \text{Mn}$  case, both GGA and GGA+U calculations can predict the ground state to be the AFM -II configuration, consistent with other studies.<sup>13</sup> Three d electrons on the  $\text{Mn}^{4+}$  ion occupy the three lower Hubbard bands with the upper ones empty as shown by the DOS in Figs. 8(c) and 8(d). In the calculated spectrum with  $E_{\perp c}$ , the optical gap comes from

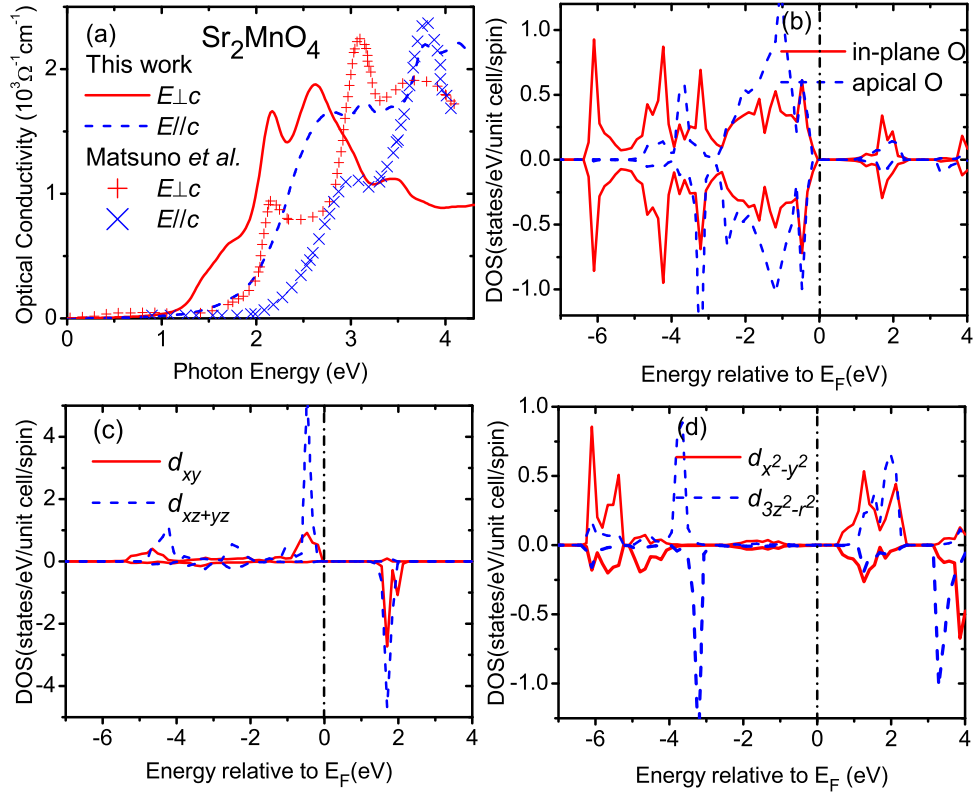


FIG. 8: (color online) (a) The experimental (symbols, from Ref. 5) and calculated (lines) optical conductivity spectra for  $\text{Sr}_2\text{MnO}_4$  in the AFM-II state within the GGA, and the corresponding partial DOS for (b) in-plane (solid) and apical (dashed) oxygen 2p bands and (c)  $t_{2g}$  and (d)  $e_g$  bands of Mn 3d electrons. The vertical dash-dotted line indicates the Fermi energy level.

the transition between the occupied in-plane oxygen 2p states and the empty Mn  $d_{x^2-y^2}$  orbital around 1.0 eV. Such a transition also contributes to the first shoulder around 1.5 eV, and this shoulder corresponds to the first peak in the experimental spectrum. The narrow peak around 2.2 eV in the calculated  $E_{\perp c}$  spectrum can be interpreted from panel (c) as the intersite  $d-d$  transition, which is not discussed in the experimental measurements.<sup>5</sup> The peak around 2.6 eV is due to the transition from the in-plane oxygen 2p bands to the  $t_{2g}$  and  $d_{x^2-y^2}$  orbitals near 2.0 eV, which corresponds to the second peak in the experimental spectrum. When  $E_{\parallel c}$ , the transition from the apical oxygen 2p bands to the Mn empty  $d_{3z^2-r^2}$  orbital contributes most of the peaks around 2.75 eV and 3.75 eV in the calculated spectrum.



#### IV . C O N C L U S I O N

For a series of layered perovskites  $\text{Sr}_2\text{M O}_4$  ( $\text{M} = \text{Ti}, \text{V}, \text{Cr},$  and  $\text{Mn}$ ), their electronic structures and the optical conductivity spectra are studied by first principles calculations within the GGA and GGA+U. The GGA calculation could successfully predict the ground state for  $\text{M} = \text{Ti}$  and  $\text{Mn}$ , but failed for  $\text{M} = \text{V}$  and  $\text{Cr}$ . In these two strongly correlated  $t_{2g}$  systems, GGA+U calculations show that the AFM-II state will have the lowest total energy when  $U$  is larger than a critical value  $U_c$ . But the optical conductivity spectra indicate that in both cases,  $U_c$  is overestimated. A analysis indicates that some cooperative changes in the ligand field such as JT or some other lattice distortions could reduce the  $U_c$  value. These changes in the electron-lattice interaction will induce further splitting of the degenerate  $t_{2g}$  orbital just as  $U$  does, which is shown to be critical for the metal-insulator transition and stabilization of AFM-II configuration in these systems. In the  $\text{M} = \text{V}$  case, since the geometric structure in bulk or thin films is well comparable with the theoretical one and nearly has no orthorhombic distortion, such a kind of additional contribution from lattice distortion seems unlikely. In  $\text{Sr}_2\text{CrO}_4$ , it has quite a large orthorhombic deviation from tetragonal symmetry in samples and a simple JT distortion is demonstrated to be quite efficient in decreasing the  $U_c$  value although this may not be the real distortion in samples. Further first-principles study of the orthorhombic distortion effects needs much detailed experimental geometric information, for which more experimental efforts are expected.

Acknowledgments

The authors thank the staff of the Center for computational Materials Science at the IMR for their support and the use of Hitachi SR8000/64 supercomputing facilities. H.M.W. acknowledges the critical reading of this work by J. Matsuno and valuable discussion with Zhijian Wu and P. Murugan. X.G.W. acknowledges support from the Natural Science Foundation of China under Grant No. 10304007 and National Key Projects for Basic Researches of China under Grant No. 2006CB0L1002.

---

Corresponding author Electronic address: hongming@imr.edu

- <sup>1</sup> See, for example, M. Imada, A. Fujimori, and Y. Tokura, *Rev. Mod. Phys.* **70**, 1039 (1998).
- <sup>2</sup> Nicola A. Spaldin and Manfred Fiebig, *Science*, **309**, 391 (2005).
- <sup>3</sup> Colossal Magnetoresistive Oxides, edited by Y. Tokura (Gordon and Breach Publishers, New York, 1999).
- <sup>4</sup> Yoshinori Tokura, *Physics Today* **56** (7), 50 (2003).
- <sup>5</sup> J. Matsuno, Y. Okimoto, M. Kawasaki, and Y. Tokura, *Phys. Rev. Lett.* **95**, 176404 (2005).
- <sup>6</sup> Yoshiki Imai, Igor Solovyev, and Masatoshi Imada, *Phys. Rev. Lett.* **95**, 176405 (2005).
- <sup>7</sup> B. L. Chamberland, *Solid State Commun.* **5**, 663 (1967).
- <sup>8</sup> Y. Maeno, H. Hashimoto, K. Yoshida, S. Nishizaki, T. Fujita, J. G. Bednorz, and F. Lichtenberg, *Nature (London)* **372**, 532 (1994).
- <sup>9</sup> J. Matsuno, Y. Okimoto, Z. Fang, X. Z. Yu, Y. Matsui, N. Nagaosa, M. Kawasaki, and Y. Tokura, *Phys. Rev. Lett.* **93**, 167202 (2004).
- <sup>10</sup> I. V. Solovyev, *Phys. Rev. B* **73**, 155117 (2006); **74**, 054412 (2006).
- <sup>11</sup> W. E. Pickett, D. Singh, D. A. Papaconstantopoulos, H. Krakauer, M. Cyrot and F. Cyrot-Lackmann, *Physica C* **162-164**, 1433 (1989).
- <sup>12</sup> D. J. Singh, D. A. Papaconstantopoulos, H. Krakauer, B. M. Klein and W. E. Pickett, *Physica C* **175**, 329 (1991).
- <sup>13</sup> J. L. Wang, Zhi Zeng, and Q. Q. Zheng, *J. Magn. Magn. Mater.* **226-230**, 1048 (2001).
- <sup>14</sup> K.-W. Lee and W. E. Pickett, *Phys. Rev. B* **73**, 174428 (2006).
- <sup>15</sup> J. P. Perdew, J. A. Chevary, S. H. Vosko, K. A. Jackson, M. R. Pederson, D. J. Singh, and C. Fiolhais, *Phys. Rev. B* **46**, 6671 (1992); *ibid.*, **48**, 4978 (1993).
- <sup>16</sup> Hongming Wang, Xiangang Wan, Jian Zhou, and Jinming Dong, *Eur. Phys. J. B* **35**, 217 (2003).
- <sup>17</sup> G. Kresse and J. Hafner, *Phys. Rev. B* **47**, R558 (1993); G. Kresse and J. Hafner, *ibid.* **49**, 14251 (1994); G. Kresse and J. Furthmüller, *Comput. Mat. Sci.* **6**, 15 (1996); *Phys. Rev. B* **54**, 11169 (1996).
- <sup>18</sup> G. Kresse and D. Joubert, *Phys. Rev. B* **59**, 1758 (1999).
- <sup>19</sup> S. L. Dudarev, G. A. Botton, S. Y. Savrasov, C. J. Humphreys, and A. P. Sutton, *Phys. Rev. B* **57**, 1505 (1998).
- <sup>20</sup> B. Adolph, J. Furthmüller, and F. Bechstedt, *Phys. Rev. B* **63**, 125108 (2001).
- <sup>21</sup> <http://www.freeware.vasp.de/VASP/>.
- <sup>22</sup> Peter E. Blochl, O. Jepsen, O. K. Andersen, *Phys. Rev. B* **49**, 16223 (1994).

- <sup>23</sup> Craig J. Fennie, and Karin M. Rabe, *Phys. Rev. B* 68, 184111 (2003).
- <sup>24</sup> R. M. Dreizler and E. K. U. Gross, *Density Functional Theory, An Approach to the Quantum Many-Body Problem* (Springer-Verlag, Berlin, 1990).
- <sup>25</sup> M. Cyrot, B. Lambert-Andron, J. L. Soubeyrou, M. J. Rey, Ph. Dehauht, F. Cyrot-Lackmann, G. Fourcaudot, J. Beille and J. L. Tholence, *J. Solid State Chem.* 85, 321 (1990); M. J. Rey, Ph. Dehauht, J. C. Joubert, B. Lambert-Andron, M. Cyrot and F. Cyrot-Lackmann, *J. Solid State Chem.* 86, 101 (1990).
- <sup>26</sup> V. I. Anisimov, I. A. Nekrasov, D. E. Kondakov, T. M. Rice, and M. Sigrist, *Eur. Phys. J. B* 25, 191 (2002).
- <sup>27</sup> H. Sawada and K. Terakura, *Phys. Rev. B* 58, 6831 (1998).
- <sup>28</sup> A. Nozaki, H. Yoshikawa, T. Wada, H. Yamachi, and S. Tanaka, *Phys. Rev. B* 43, 181 (1991).
- <sup>29</sup> Xiangang Wan, M. Kohno, and X. Hu, *Phys. Rev. Lett.* 94, 087205 (2005).
- <sup>30</sup> J. S. Lee, M. W. Kim, and T. W. Noh, *New J. Phys.* 7, 147 (2005).
- <sup>31</sup> M. Braden, G. Andre, S. Nakatsuji, and Y. Maeno, *Phys. Rev. B* 58, 847 (1998).
- <sup>32</sup> Zhong Fang, Kiyoyuki Terakura, and Naoto Nagaosa, *New J. Phys.* 7, 66 (2005).